JOURNAL OF BIOMEDICAL OPTICS 3(4), 437–445 (OCTOBER 1998)

COMPUTATIONAL AND *IN VIVO* INVESTIGATION OF OPTICAL REFLECTANCE FROM HUMAN BRAIN TO ASSIST NEUROSURGERY

Maureen Johns,[†] Cole Giller,[‡] and Hanli Liu[†]

[†]University of Texas Arlington/Southwestern Medical Center at Dallas, Joint Program of Biomedical Engineering, Arlington, Texas 76019; [‡]University of Texas Southwestern Medical Center at Dallas, Department of Neurological Surgery, Dallas, Texas 75235-8855

(Paper JBO-191 received Feb. 6, 1998; revised manuscript received July 10, 1998; accepted for publication July 23, 1998.)

ABSTRACT

Parkinson's disease (PD) is a chronic, progressive disease involving the globus pallidus (GP), which is a gray matter mass, surrounded by white matter deep within the brain. During a neurosurgery procedure, a thin probe is inserted into the GP to create a lesion that often relieves the cardinal symptoms of PD. The goal of this study is to develop an optical method to accurately locate the GP border. In theory, Monte Carlo simulations were performed to predict the optical reflectance from brain tissue. In experiment, a portable, real-time display spectrometer with a fiber optic reflectance probe was developed and used during human surgery. Optical reflectance values were recorded at 1 mm intervals to obtain a spatial profile of the tissue as the probe passed through regions of gray and white matter. The simulation and *in vivo* studies of the reflectance from the brain are in good agreement with one another. The clinical data show that the reflectance from gray matter is approximately 50% or less than that from white matter between 650 and 800 nm. A slope algorithm is developed to distinguish gray and white matter *in vivo*. This study provides previously unknown optical reflectance of the human brain. © *1998 Society of Photo-Optical Instrumentation Engineers.* [S1083-3668(98)00904-6]

Keywords absorption; fiber optic applications; optical properties; reflectance; spectroscopy.

1 INTRODUCTION

Interests in using optical methods for physiological-condition monitoring and cancer diagnostics have increased in recent years due to their simplicity, low cost, and low risk. Mourant et al.[1] have used elastic scattering spectroscopy with a portable, fiber-optic spectrometer to diagnose cancerous tissue in human gastrointestinal tracts. The principle behind this method is that the scattering properties of cancerous and healthy tissue are different. Similarly, the absorption and scattering properties of gray matter and white matter of the brain should also be different. This difference can be used as a diagnostic tool for mapping the boundary between gray and white matter. The goal of this paper is to demonstrate the feasibility of using optical reflectance measured *in vivo* to identify gray matter, white matter, and the boundary between the two tissues for guiding brain surgery.

The basal ganglia, structures deep within the brain composed mostly of gray matter, are surrounded by laminae of white matter. Damage to the basal ganglia is associated with involuntary movements and widespread changes in muscle tone. An important mass of gray matter that forms the major output structure of the basal ganglia is known as the globus pallidus (GP), which lies deep within the brain and is surrounded by white matter. Abnormalities of the GP are associated with tremors in Parkinson's disease (PD) patients.[2] Surgical treatments, such as a pallidotomy, are an option for some Parkinson's patients; however, identification of the GP boundary is difficult.

During a pallidotomy, a thin probe is inserted into the GP to create a small lesion with radio frequency current. The optimal lesion size is unknown; lesions are generally placed in the posterior ventral GP, near the optic nerve.[3,4] These lesions help relieve the difficult symptoms (specifically, tremors) associated with PD. The difficulty of this procedure involves precise mapping of the GP border. A lesion miscalculation (i.e., too deep or too medial) could cause permanent damage, such as blindness or paralysis, respectively. However, an ongoing debate exists regarding alternate methods to use for accurate localization of the GP.[5]

During the past two decades, limited articles have been published that discuss the optical properties of human brain tissue, either *in vitro* or *in vivo*. Sterenborg et al.[6] measured the absorption and scattering coefficients of gray and white matter

Address all correspondence to Hanli Liu. Tel: (817) 272-2054; Fax: (817) 272-2251; E-mail: hanli@utarlg.uta.edu

slices from a post mortem human brain in the wavelength range from 400 to 1100 nm. Similarly, van der Zee et al.[7] measured the reflectance and transmittance of gray and white matter in post mortem neonatal and adult human brain tissue in the wavelength range from 500 to 1000 nm. Since post mortem tissues contain decreased blood volume and show signs of necrosis, it is possible that post mortem samples may provide variable results versus *in vivo* samples. In addition, Wilson et al.[8–10] have reported on the penetration depth of light in normal and malignant human brain tissue *in vivo*. Those studies were performed during photodynamic therapy, so only selected wavelengths were used.

Boyer et al.[11,12] and Mourant et al. have investigated elastic scattering spectroscopy using scattering spheres *in vitro* and on human organs *in vivo*, with an instrument consisting of a light source, optic delivery and collection fibers, a spectrometer, and a CCD detector array. The system wavelength range was from 300 to 750 nm. Studies on human brain tissue, either *in vivo* or *ex vivo*, have not been reported using such an instrument. In this paper, we first show our Monte Carlo calculations, simulating the reflectance signal from the human brain. Then we will describe the experimental setup, which is similar to the system used by Boyer et al., followed by experimental results obtained during neurosurgeries. Finally, we will discuss the consistency between the simulations and experimental data, develop a slope algorithm to differentiate gray and white matter, and then draw conclusions.

2 COMPUTATIONAL SIMULATIONS

Since the separation of the source and detector is about 300–500 μm in our case, diffusion theory would not be valid. We employ Monte Carlo simulations to predict the optical reflectance from the human brain. The simulation code was provided by Wang and Jacques through the internet.[13] Our input parameters used for the simulations are as follows: the average index of refraction (n) for tissues was 1.38,[14] the mean cosine of the scattering angle (g) for tissues was 0.9, and the tissue sample thickness (d) was chosen as 10 cm. The simulations were performed with a spatial step size of 0.05 mm (50 μm) and a maximum detection radius of 1.5 mm (1500 μm). The input scattering and absorption coefficients (μ_s and μ_a) were chosen based on the following calculations.

Matcher et al.[15] presented a linear function to calculate the reduced scattering coefficient (μ_s') for the human head with $\mu_s'(\lambda)=a\lambda+b$, where $a=-6.5\times10^{-4}$ mm^{-1} nm^{-1}, $b=1.45$ mm^{-1}, and λ is wavelength in nm. Using this equation, we obtain the scattering coefficient as $\mu_s=\mu_s'/(1-g)$. Furthermore, Zijlstra et al.[16] generated a table of extinction coefficients of oxyhemoglobin and deoxyhemoglobin for adult hemoglobin in the wavelength range

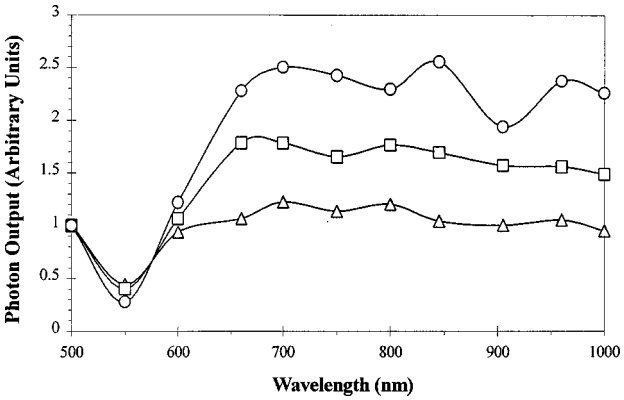

Fig. 1 Monte Carlo simulations of optical reflectance spectra for 100% deoxygenated Hb. The unit of the ordinate axis is the number of photons per area, and the spectra were normalized to the reflectance value at 500 nm. Open triangle represents 0.05 cm source-detector separation. Open square represents 0.10 cm source-detector separation. Open circle represents 0.14 cm source-detector separation.

from 450 to 1000 nm. It is also known that an average value of the absorption coefficient measured noninvasively on the human head is approximately 0.1 cm^{-1} at 800 nm, which most likely includes all effects of blood vessels, capillaries, and the tissue background. To be consistent with this known value in the simulation, we assumed the hemoglobin concentration to be 8 mM with human tissue containing 5.5% blood with 45% hematocrit. This leads to an effective hemoglobin concentration of [8 mM$\times$0.055$\times$0.45=] 2 mM in the detected volume. The absorption coefficient used in the simulation is equal to the product of the 2 mM hemoglobin concentration and the tabulated extinction coefficients of pure hemoglobin given by Zijlstra et al. (with a conversion factor of 2.3 to convert between log 10 base and ln e base). This step ensures that values of the absorption coefficient used in the simulation are close to those for blood-containing tissues. These μ_s and μ_a values were chosen to simulate brain tissue in general, and gray and white matter were simulated by having high and low absorption, respectively.

Figures 1 and 2 show simulated optical reflectance (shown as photon output) for tissues containing 0% and 100% oxygenated hemoglobin, respectively. They both display a noticeable decrease in signal intensity at 550 nm. This corresponds to the absorption peak of both deoxygenated and oxygenated hemoglobin.[14] Oxyhemoglobin simulations (Figure 2) do not show double peaks since the spectral resolution of the simulations is not high enough to observe the double-peak feature. However, the purpose of these simulations was not to detect small details within the spectra but to observe the overall shape. The curves in both figures also show a slow decay at longer wavelengths that mirror scattering behavior.

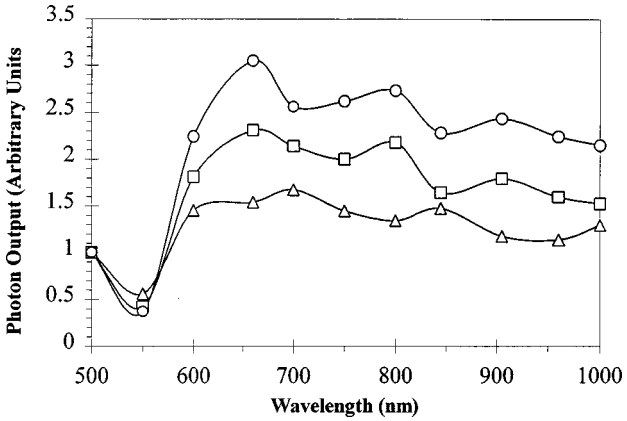

Fig. 2 Monte Carlo simulations of optical reflectance spectra for 100% oxygenated Hb (HbO_2). The unit of the ordinate axis is the number of photons per area, and the spectra were normalized to the reflectance value at 500 nm. Open triangle represents 0.052 cm source-detector separation. Open square represents 0.10 cm source-detector separation. Open circle represents 0.14 cm source-detector separation.

In order to clarify the pure scattering feature, additional Monte Carlo simulations were performed and compared under two conditions. The first set of the simulations considers only scattering effects with the absorption coefficient chosen to be zero. The second set of the simulations uses both scattering and absorption coefficients as input parameters. The simulated results are given in Figure 3. This shows that in the case of pure scattering ($\mu_a = 0$), the simulated reflectance signal has a slow decay feature, which is similar to that of the input scattering parameters. On the other hand, with both scattering and absorption, the simulated reflectance displays a significant decrease in output signal at 550 nm, i.e., at the hemoglobin absorption peak, and also displays slow decay characteristics from 700 to 1000 nm.

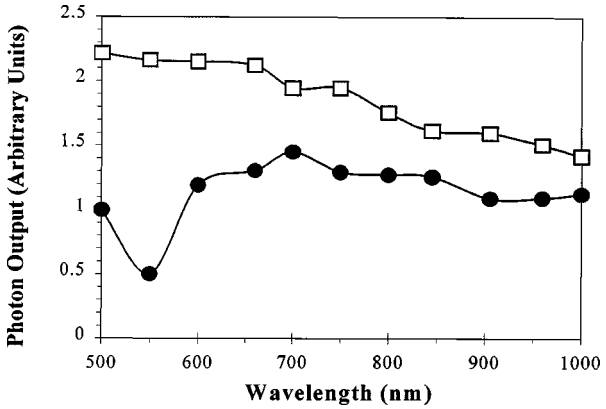

Fig. 3 Monte Carlo simulation results showing effects of scattering and absorption (represented by filled circle) and effects of scattering only (represented by open square). The unit of the ordinate axis is the number of photons per area, and the spectra were normalized to the reflectance value with both effects of absorption and scattering at 500 nm.

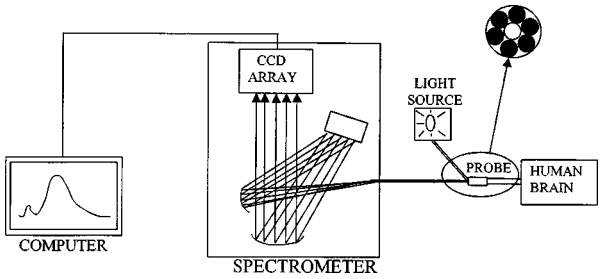

Fig. 4 Experimental setup. Refer to text for detailed explanation.

3 MATERIALS AND METHODS

3.1 EXPERIMENTAL SETUP

Prior to surgery, the stereotactic frame was secured to the patient's head. This device provides stable fixation to allow accurate placement of the surgical radio frequency probe as well as our fiber optic probe. Our probe has similar dimensions to those of the surgical probe and can therefore be used with the existing surgical equipment.

As shown in Figure 4, the experimental studies used a custom designed, portable, real-time display spectrometer (SD2000, Ocean Optics, Inc.) with a fiber optic probe of 1.5 mm in diameter to obtain the reflected signals from the human brain during surgery. The spectrometer was grated for use in the wavelength range from 500 to 1000 nm. The fiber optic probe measured two meters in total length. The first 20 cm was made of hypoallergenic stainless steel, and the remaining length of the fiber bifurcated into two 1 m segments. One side connected to the tungsten halogen light source (LS-1, Ocean Optics, Inc.) and the other to the spectrometer. The probe used during the clinical measurements had one light fiber in the center surrounded by six collection fibers. All fibers were 200 μm in diameter with a core-to-core separation of approximately 200 μm. This configuration was chosen to prevent the detector from being saturated based on results obtained from laboratory model studies. Six collection fibers are bundled together into a single fiber format and then coupled into the spectrometer through a SMA connector. With 200 μm core-to-core separation, we detect the volume of brain material approximately 100–200 μm below the probe with a diameter of 400 μm centered at the location of the source fiber tip. The brain volume contributed to the backscattered detection has a doughnut shape with a small hollow near the source fiber tip. The accurate detection depth and the backscattered intensity depend on both the absorption and scattering features of the detected brain volume. Higher absorption causes a shallower detection depth and a decrease in backscattered intensity, while higher scattering leads to a deeper detection depth and an increase in backscattered intensity.

Table 1 Patient statistical information for *in vivo* experiments.

Experiment No.	Surgical procedure	Age	Sex
1	Lt. temporal lobectomy	40	F
2	Lt. stereotactic pallidotomy w/ CT guidance	56	M
3	Lt. stereotactic thalamotomy w/ CT guidance	34	F
4	Lt. stereotactic pallidotomy w/ CT guidance	70	F
5	Lt. temporal lobectomy	22	F
6	Lt. stereotactic pallidotomy w/ CT guidance	46	M
7	Lt. stereotactic pallidotomy w/ CT guidance	67	M

3.2 CALIBRATION

In principle, a reflected signal can be calculated as $R = (\text{signal-dark})/(\text{reference-dark})$, where ''dark'' results from all ambient light, and ''reference'' includes all effects of light source, fiber optics, and any other background excluded from the tissue studied. We assumed that the reference signal would affect all of our clinical curves equally; therefore, we conducted our studies in two ways: (1) all graphs obtained from clinical data were calculated using only (signal-dark) by neglecting the reference signal and, (2) to be accurate, the clinical data curves were reanalyzed by including the reference signal in the denominator. The dark values for the reference were very small compared to the reference values and, therefore, neglected.

To measure the reference signal, we placed two fibers facing one another: one fiber was connected to the spectrometer, the other fiber was connected to the light source. As light traveled through the incident fiber of one probe, the light immediately entered the detection fiber of the second probe and was recorded by the spectrometer. This reading produced a reference curve that included the effects of the light source and the fiber on the detected reflectance signal.

3.3 PROCEDURES FOR CLINICAL MEASUREMENTS

The clinical trials were performed on human subjects that were admitted to the hospital specifically for neurosurgery not related to this study. The patient statistics for the experiments are presented in Table 1.

For all of the experiments, the measurement procedure involved placing the probe against the surface of the brain during surgery, recording the intensity of light reflected from the tissue in the spectral range from 500 to 1000 nm, and lowering the probe deeper into the brain with 1 mm increments, until the probe reached 15 mm below the surface. This technique allowed the optical reflectance signals from both white and gray matter to be obtained as the probe passed through these tissues. Following data acquisition, the surgical probe was inserted along the same tract created by the fiber optic probe; therefore, the tissue did not suffer additional injury. All measurements were recorded with a 10 ms integration time.

During experiment Nos. 1 and 5, a section of brain tissue was scheduled to be removed. In both cases, measurements were performed on the tissue both *in vivo*, prior to excision, and *ex vivo*, immediately following excision; therefore, no harm was done to the patient's remaining healthy brain tissue. In addition, the excised tissue left behind a cavity that contained both living gray and white matter, which were visually identified. In those cases, the reflectance measurements were also taken from both tissues as well as along the boundary to obtain standard spectra of gray and white matter as references to be used as a means for comparison.

4 EXPERIMENTAL RESULTS

As noted, the goal of this research was to obtain the optical reflectance of human brain tissue with a fiber optic probe in order to help identify gray and white matter *in vivo*. The results presented in Secs. 4.1 and 4.2 are taken *in vivo* and *ex vivo*, respectively, without calibration using a reference, showing a significant difference in spectral intensities reflected from gray and white matter. Furthermore, Sec. 4.3 gives an example of calibrated results, showing good consistency between the simulations and the experimental data.

4.1 *IN VIVO* MEASUREMENTS

Two different types of measurements were taken *in vivo*. The first type involved visually identifying gray and white matter and taking a measurement after a section of brain tissue was removed. The second type involved inserting the probe into the brain, recording data, and then identifying gray and white matter based on characteristics observed in the data curves.

4.1.1 Gray and White Matter—Visually Identified

During experiment Nos. 1 and 5, a portion of brain tissue was removed for therapeutic reasons unrelated to the experiments. The excised brain tissue left behind a cavity that contained both gray and white matter. They were visually identified and reflectance measurements were taken from both tissues. The results provided a set of characteristic curves showing the optical reflectance of gray and white matter found in living, human brain tissue *in vivo*. Figure 5 shows the characteristic differences between gray and white matter obtained from experiment No. 1. White matter reflectance occasion-

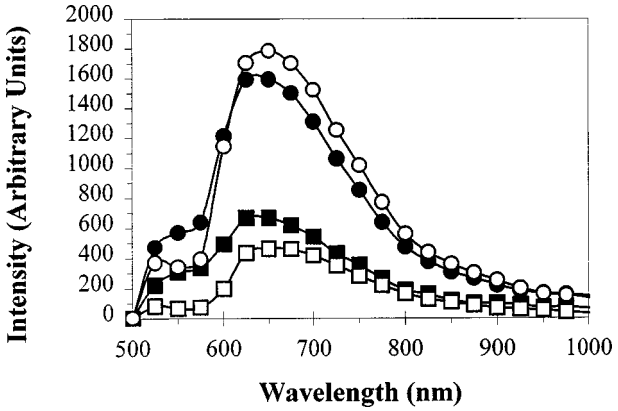

Fig. 5 Reflectance measured from visually identified living gray and white matter *in vivo* obtained during experiment No. 1. Open square represents gray matter at one location. Filled square represents gray matter at another location. Open circle represents white matter at one location. Filled circle represents white matter at another location.

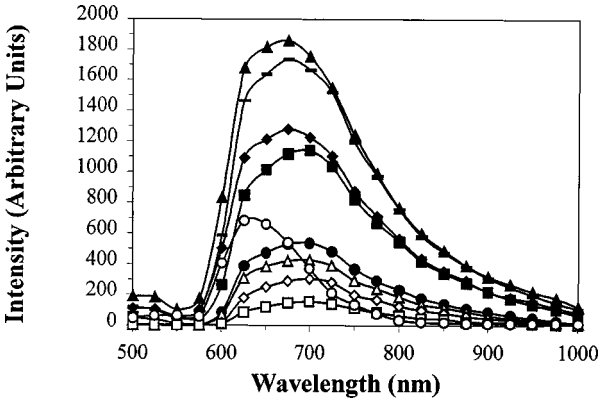

Fig. 6 Reflectance measurements taken *in vivo* consecutively during experiment No. 6 from 1 to 15 mm deep within the brain. Open circle represents 1 mm deep (W). Open square represents 2 mm deep (G). Open diamond represents 3 mm deep (B). Open triangle represents 4 mm deep (W). Filled circle represents 5 mm deep (W). Filled square represents 6 mm deep (W). Filled diamond represents 7 mm deep (W). Filled triangle represents 8 mm deep (W). Dash mark represents 15 mm deep (W). Curves taken from 9 to 14 mm deep are not shown on this graph to enhance clarity; however, they fall between the 8 and 15 mm curves shown.

ally shows a dip at 550 nm. The presence of this dip depends upon the amount of blood present, which influences absorption by hemoglobin. In general, the reflected signal from white matter has a prominent peak at approximately 650 nm. The reflectance from gray matter has a similar peak at 650 nm; however, the maximum value from gray matter is approximately 50% or less than that of white matter.

4.1.2 Gray and White Matter—Experimentally Identified

During all of the experiments, the probe was stereotactically fixed above the surgical region. The probe was inserted in 1 mm increments to a depth of 15 mm below the surface of the brain. Optical reflectance measurements were recorded at each 1 mm step to obtain a spatial profile of the tissue as the probe passed through regions of gray and white matter.

All seven experiments produced curves showing a consistent spectral shape from 600 to 1000 nm. The experimental graphs plot wavelength in nm along the x axis and reflected intensity in arbitrary units along the y axis. Data obtained between 500 and 600 nm were variable. The amount of blood present influenced the degree of signal absorption at 550 nm and, therefore, influenced the spectral shape between 500 and 600 nm. As mentioned earlier, higher scattering in the brain leads to a deeper detecting depth and to an increase in backscattered intensity. As shown in Figure 6, the backscattered intensity increases abruptly between probe positions of 5 and 6 mm. This indicates that scattering property is increasing quite largely between these two positions, although both of them are within the white matter category. This suggests that scattering properties within white matter are not necessarily the same, increasing gradually from the boundary toward the deep region of white matter. Figure 6 shows an example (from experiment No. 6) of the overall spectral shape and type of tissue determined for each incremental curve (G: for gray matter; B: for boundary region; W: for white matter). The slope algorithm used to assign G, B, or W to each curve will be discussed in Sec. 5.3.

The results shown here are obtained according to the slope algorithm. However, the 1-mm-deep curve identified as white matter is most likely untrue. In general, the outer 2 to 3 mm of cortex is gray matter, which contains cell bodies and produces decreased reflectance. White matter, which begins approximately 3 mm deep, contains myelin and yields increased reflectance. Although white matter could, in some cases, be found at 1 mm deep, the unusually high intensity curve may also be due to excess fluid secreted from brain tissue (such as from cerebrospinal fluid) at the measurement location. This fluid has very little absorption and may lead to ''a tunneling effect'' for the light to be detected, thereby causing a noticeably greater reflectance. Assuming the 1-mm-deep curve is actually from gray matter, these curves show a 2 mm gray matter region, a thin 1 mm boundary region followed by a large white matter region (>12 mm thick). The curves from 2 to 5 mm deep have a fairly low reflected intensity. However, these values are consistent with those observed from visually identified living gray matter *in vivo* (Figure 5).

4.2 *EX VIVO* MEASUREMENTS

As stated, during experiment Nos. 1 and 5, a tissue section was removed from the brain. Similarly to *in vivo* recognition, gray and white matter could be visually identified within the excised tissue. Measurements were taken on *ex vivo* gray and white

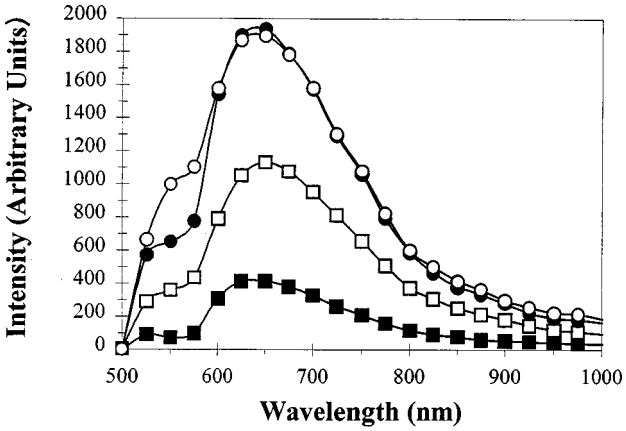

Fig. 7 Reflectance measurements taken from *ex vivo* tissue during experiment No. 1. Filled square represents gray matter at one location. Open square represents gray matter at another location. Filled circle represents white matter at one location. Open circle represents white matter at another location.

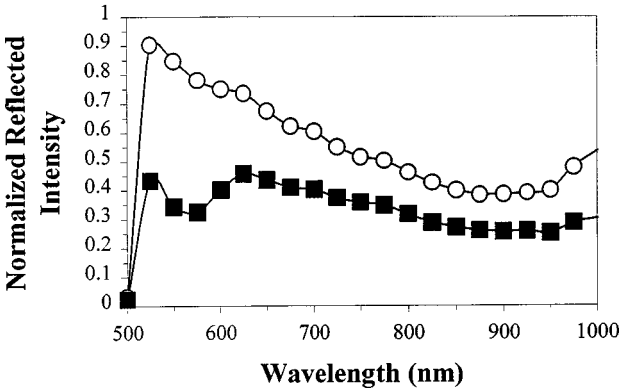

Fig. 8 Calibrated reflectance obtained by dividing *in vivo* curves (from experiment No. 1) by reference light curve. Filled square represents 3 mm deep curve after calibration. Open circle represents 14 mm deep curve after calibration.

matter. Figure 7 provides the corresponding curves, which seem similar in spectral shape and intensity to those obtained *in vivo* from visually identified tissues shown in Figure 5.

During experiment No. 1 and 5, both sections of *ex vivo* tissue were analyzed by pathology following the optical measurements. Based on the pathology results from experiment Nos. 1 and 5, cortical gray matter thickness ranged from 2 to 5 mm. This region contained swirls of gray matter mixed with superficial white matter within the superficial 1 to 2 cm. This may explain the variability of the surface data. In one instance, the pathology results showed that two gyri were back to back forming a total gray matter depth of 9.1 mm. This also explains the variability observed during the optical experiments. In general, the pathological results support the data obtained from the reflectance measurements.

4.3 CALIBRATED RESULTS

Since the results obtained in the above section were not calibrated with a reference, they include effects from the light source, fiber optic, and instrument. In order to compare the experimental data with the simulation results given in Sec. 2, we obtained calibrated reflectance by dividing the measured curve by the reference curve. One example is shown in Figure 8, where two calibrated curves measured 3 and 14 mm below the brain surface are plotted. It is known that a 3 mm location below the brain surface roughly correlates to the boundary region between gray and white matter, and that a 14 mm location in the brain roughly correlates to white matter (see Sec. 5.3 for algorithm details). Figure 8 shows that the spectral shape of the calibrated reflectance from 14 mm location exhibits a slow decay feature between 500 and 900 nm. This is characteristic of light scattering by tissue (i.e., white matter), as predicted by the Monte Carlo simulations in Figure 3. In addition, the calibrated reflectance from 3 mm location in this figure has a similar feature from 650 to 900 nm and has a signal decrease at 550 nm. The former aspect stems from light scattering by gray matter, whereas the latter aspect is due to hemoglobin absorption at 550 nm, as also demonstrated in the Monte Carlo simulations in Figure 3. Changes in magnitude of the drop at 550 nm have been observed in different cases and can be attributed to the local concentration of hemoglobin in the measured area. In comparison to the uncalibrated spectra, the calibrated results allow us to study the scattering and absorption properties of the human brain more quantitatively and reveal good consistency between the simulations and the calibrated reflectance.

5. DISCUSSION

5.1 COMPARISON BETWEEN *IN VIVO* AND *EX VIVO* RESULTS

Figure 9 shows two gray matter curves taken *in vivo* and two curves *ex vivo*, all of the which are normalized to their maximum values. This figure shows that the reflectance measured from human gray matter both living and 5–10 min after excision from the brain have similar spectral properties in the wavelength range of 650–1000 nm. However, the spectral features between 500 and 600 nm vary, perhaps due to the variation of blood contents in the measured area. Similar behaviors were also observed from white matter both *in vivo* and *ex vivo* measurements. This observation suggests that when a piece of brain tissue is removed from its living condition, the scattering properties of the removed brain do not change immediately, whereas the absorption properties of the specimen depend greatly on the local blood content left on the tissue.

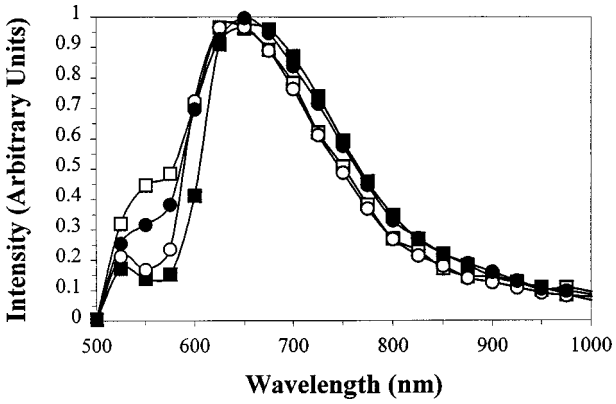

Fig. 9 *In vivo* and *ex vivo* gray matter curves from location No. 1, experiment No. 1 normalized to their maximum values. Open square represents one gray matter location taken *in vivo*. Filled square represents another gray matter location taken *in vivo*. Open circle represents one gray matter location taken *ex vivo*. Filled circle represents another gray matter location taken *ex vivo*.

5.2 OPTICAL PROPERTIES OF LIVING BRAIN TISSUE

In Sec. 4.3, we illustrate good consistency between the Monte Carlo simulations and the calibrated curves. This consistency indicates that the assignment of input parameters in simulations for optical properties of the brain is reasonable. The input scattering coefficients were based on noninvasive measurements performed on human heads, including effects from the scalp and skull.[15] By combining a recently developed algorithm[17] with the calibrated experimental results, it is possible to extract the scattering and absorption properties of living gray and white matter of the human brain, which have been unavailable prior to this study. In the near future, one goal of this study is to quantitatively obtain optical properties of living brain tissue based on our mm scale, reflectance measurements.

Although the calibrated results are valuable in studying optical properties, the spectral features between gray and white matter cannot be clearly distinguished, as shown in Figure 8. The curves from both 3 and 14 mm deep locations have slow decay features with just slightly different slopes between 650 and 900 nm. The signal drop at 550 nm can appear in either curve with variable magnitudes, depending on the local blood content. Therefore, we need to develop a quick and efficient algorithm to differentiate gray and white matter.

5.3 DEVELOPMENT OF SLOPE ALGORITHM

Concerns prior to experimentation include: (1) whether gray and white matter can be properly identified *in vivo*, and (2) whether it is possible to replicate the data from one experiment to the next. Based on Figure 6, as well as similar curves obtained from other experiments, the most noticeable difference in reflectance between gray and white matter was the variation in slope between 700 and 850 nm. In order to create an effective algorithm using the slope of each curve, the solution must be one that can be applied quickly and accurately while in the operating room to identify the tissues as the probe passes through.

Since the intensities of measured signals may vary from case to case, the absolute slopes of such reflectance are difficult to compare from case to case or from person to person. A slope algorithm is developed as follows: after choosing a fixed reflectance curve as a reference, we calculate the slopes of all measured reflectance spectra and then divide those slopes by the slope of the chosen reference. The ratios of the slopes between the measured signals and reference are characteristic of gray and white matter, enabling us to differentiate gray matter, white matter, and their boundary. In order to test this slope algorithm, calculations are first performed on data obtained *in vivo* and *ex vivo* from visually identified gray and white matter during experiment Nos. 1 and 5. The slopes of all curves are calculated between 700 and 850 nm since within this wavelength range there are no absorption bands, and the curves are fairly linear. The slope value from the first set of gray matter taken *in vivo* is chosen as the fixed reference. This value is selected simply because the first data point might also be chosen as the reference during a surgical procedure. There is no significant difference between slope values ($\alpha = 0.05$, $p < 0.001$) among the gray matter (and white matter) curves measured *in vivo* and *ex vivo*; therefore, all gray matter curves (and all white matter curves) were pooled, respectively. The complete table of slope results is presented in Table 2. It shows that the standardized values, i.e., ratios of the slopes, calculated for gray and white matter are statistically different ($\alpha = 0.05$, $p < 0.001$).

Based on these data, the means (μ) and standard deviations (σ) of the standardized values from gray and white matter are summarized in Table 3. This table shows that the standardized values of gray matter obtained in both *in vivo* and *ex vivo* measurements range from 0.585 to 1.051, and those in white matter measurements range from 2.189 to 2.921. Based on these calculated values, the following numerical limits of the standardized slopes are determined to help identify gray matter and white matter tissues: $0.0 <$ gray matter < 1.10, $2.00 <$ white matter.

5.4 BRAIN TISSUE IDENTIFICATION USING SLOPES

Similar calculations were performed to experimentally identified brain tissue by applying the slope algorithm presented in Sec. 5.3. In general, 2 mm deep within the brain is gray matter and does not contain fluid from the surface that could interfere with the measurement. Therefore, the 2 mm curve is chosen as the reference curve. This is the method

Table 2 The top box shows slope values from data curves obtained from visually identified gray and white matter, both *in vivo* and *ex vivo*. The bottom box shows the slope values divided by the reference value (gray 1, *in vivo*). Note: Gray1 *ex vivo* and Gray1 *in vivo*, for example, were not taken at the same location on the brain tissue. Numbers 1 and 2 are used only to designate the first and second recorded data points taken from each tissue type.

	Slope values	
	EXP No. 1	EXP No. 5
Gray1, *ex vivo*	−2.590	−3.145
Gray2, *ex vivo*	−3.219	−1.349
Gray1, *in vivo*	−3.471	−2.832
Gray2, *in vivo*	−2.665	−1.455
White1, *ex vivo*	−8.167	−8.280
White2, *ex vivo*	−9.634	−8.476
White1, *in vivo*	−8.413	−5.837
White2, *in vivo*	−9.717	−5.973
	Slope/slope@reference	
	EXP No. 1	EXP No. 5
Gray1, *ex vivo*	0.746	1.110
Gray2, *ex vivo*	0.927	0.476
Gray1, *in vivo*	1.000	1.000
Gray2, *in vivo*	0.768	0.514
White1, *ex vivo*	2.353	2.924
White2, *ex vivo*	2.776	2.993
White1, *in vivo*	2.424	2.061
White2, in vivo	2.800	2.109

that was used to assign tissue types for Figure 6 and all other measurements. Tissue identification in this manner has been supported by the pathology results. Since the reference curve plays an important role in the algorithm, it is important to choose the reference carefully. Small amounts of surface fluid can cause significant errors; therefore, in order to obtain a more reliable reference value, it is recommended that multiple readings at a 2 mm depth be recorded, and that the average slope of these multiple curves be used as the reference slope. The burr hole that had been drilled through the skull is ~1.5 cm in diameter, large enough to obtain reflectance measurements at several different tissue locations. In addition, it is suggested that a second algorithm be implemented in conjunction with the slope algorithm to obtain more accurate/reliable results. The area under the spectral curves may prove

Table 3 This statistical table shows the mean and standard deviation values of the standardized slopes for gray and white matter data curves obtained both *in vivo* and *ex vivo*.

Tissue type	*n*	Mean (μ)	Standard deviation (σ)	$\mu-\sigma$, $\mu+\sigma$
Gray matter, *ex vivo*	4	0.815	0.270	0.545, 1.085
Gray matter, *in vivo*	4	0.820	0.232	0.589, 1.052
Total gray (*ex+in vivo*)	8	0.818	0.233	0.585, 1.051
White matter, *ex vivo*	4	2.761	0.287	2.474, 3.048
White matter, *in vivo*	4	2.349	0.341	2.007, 2.690
Total white (*ex+in vivo*)	8	2.555	0.366	2.189, 2.921

to be a useful tool. Although this analysis has not been performed, the area under any given curve coupled with the standardized slope value for that curve may provide a more complete analysis.

During experiment Nos. 1 and 5 the surgical procedure was a temporal lobectomy. During these experiments a larger portion of skull was removed, thereby exposing a greater portion of brain. In addition, the patient was under general anesthesia. These two factors may influence the blood volume within the brain tissue, which, in turn, could affect the reflectance measurements. Further study is needed for this regard.

5.5 USEFULNESS OF THIS STUDY

Various publications[14,18] have reported measurements for animal brains. Due to vascular differences between animal and human, it is difficult to apply these reported animal studies to the human brain. Therefore, this study provides valuable information on the optical reflectance of living human brain tissue.

Although the results obtained in this study are from the surface of the brain to 15 mm deep within the brain, the principle behind the slope algorithm developed in this study can be applied to other deep regions within the brain. As the instrumentation and analytic methods continue to improve, this method for identifying gray and white matter *in vivo* may prove to be a valuable tool for both pallidotomy and pallidal stimulation.

6 SUMMARY AND CONCLUSION

Monte Carlo simulations provide an estimate of the expected results based on the approximate values entered into the simulation code. Results obtained

from the simulations and experiments are qualitatively in good agreement; therefore, the input values (g, μ_s', and μ_a) obtained from literature are reasonable to use for the living, human brain. The g value was chosen as 0.9, the generally accepted value for tissues. The scattering coefficients, μ_s, in the spectral range of 500–1000 nm were determined from noninvasive measurements of human heads. The absorption coefficients, μ_a, were based on the absorption spectrum of pure hemoglobin.

Larger reflected signals detected from white matter indicate stronger scattering features in white matter than in gray matter. The presence of a signal decrease at 550 nm in both gray and white matter measurements suggests hemoglobin is a major absorbing species in the brain, particularly in gray matter. However, other absorbers may be present, but more advanced algorithms are needed to detect their presence.

The data acquisition software code (OOIBASE) can be correlated with other software to calculate the slope of each curve during the surgical procedure. Using the numerical cutoff values for gray and white matter, a tissue profile can be determined as the optical probe is in use.

In conclusion, the computational simulations and *in vivo* studies of optical reflectance from the human brain are in good agreement with one another. The results obtained through seven *in vivo* experiments support the hypothesis that optical reflectance can be used to assist identification of gray and white matter *in vivo*. As of this writing, few articles have been published which present *in vivo* optical properties of human brain tissue. In addition to identifying gray and white matter in living tissue, this study has taken one step closer toward obtaining the optical properties of human brain tissue *in vivo*.

Since the number of samples investigated is statistically small, it would be necessary to carry out similar measurements on a large number of subjects before the reliability of the method can be ascertained and the validity of the proposed algorithm, or some alternative, established. Further work applying the measurement technique to artificial models with similar but known characteristics to those of the human brain would help to validate the technique.

Acknowledgments

The authors wish to acknowledge the 1997 Research Enhancement Program supported by the University of Texas at Arlington and The Whitaker Foundation for sponsoring this research project.

REFERENCES

1. J. R. Mourant, I. J. Bigio, J. Boyer, T. M. Johnson, J. Lacey, A. G. Bohorhoush, and M. Mellow, ''Elastic scattering spectroscopy as a diagnostic tool for differentiating pathologies in the gastrointestinal tract: Preliminary testing,'' *J. Biomed. Opt.* **1**(2), 192–199 (1996).
2. F. Johansson, J. Malm, E. Nordh, and M. Hariz, ''Usefulness of pallidotomy in advanced Parkinson's disease,'' *J. Neurology Neurosurg. Psych.* **62**, 125–132 (1997).
3. R. P. Iacono, R. R. Lonser, G. Mandybur, and S. Yamada, ''Stimulation of the globus pallidus in Parkinson's disease,'' *Br. J. Neurosurg.* **9**, 505–510 (1995).
4. L. V. Laitinen, A. T. Bergenheim, and M. I. Hariz, ''Leskell's posteroventral pallidotomy in the treatment of Parkinson's disease,'' *J. Neurosurg.* **76**, 53–61 (1992).
5. C. A. Giller, R. B. Dewey, M. I. Ginsburg, D. B. Mendelsohn, and A. M. Berk, ''Stereotactic pallidotomy and thalamotomy using individual variations of anatomic landmarks for localization,'' *Neurosurgery* **42**(1), 56–65 (1998).
6. H. J. C. M. Sterenborg, M. J. C. van Gemert, and A. J. Welsh, ''The spectral dependence of the optical properties of human brain,'' *Lasers Med. Sci.* **4**, 221–227 (1989).
7. P. van der Zee, M. Essenpreis, and D. T. Delpy, ''Optical properties of brain tissue,'' 1993 (unpublished).
8. B. C. Wilson, P. J. Muller, and J. C. Yanch, ''An update on the penetration depth of 630 nm light in normal and malignant human brain tissue *in vivo*,'' *Phys. Med. Biol.* **31**(11), 1295–1297 (1986).
9. B. C. Wilson, P. J. Muller, and J. C. Yanch, ''Instrumentation and light dosimetry for intraoperative photodynamic therapy (PDT) of malignant brain tumours,'' *Phys. Med. Biol.* **31**(2), 125–133 (1986).
10. B. C. Wilson, M. S. Patterson, and S. T. Flock, ''Indirect versus direct techniques for the measurement of the optical properties of tissues,'' *Photochem. Photobiol.* **46**(5), 601–608 (1987).
11. J. Boyer, J. R. Mourant, and I. J. Bigio, ''Theoretical and experimental investigations of elastic scattering spectroscopy as a potential diagnostic for tissue pathologies,'' *J. Opt. Soc. Am.* **21**, 265–268 (1994).
12. J. Boyer, J. R. Mourant, and I. J. Bigio, ''Monte Carlo investigations of elastic scattering spectroscopy applied to latex spheres used as tissue phantoms,'' *Proc. SPIE* **2389**, 103–112 (1996).
13. L.-H. Wang, S. L. Jacques, and L.-Q. Zheng, ''MCML—Monte Carlo modeling of photon transport in multi-layered tissues,'' *Comput. Methods Programs Biomed.* **47**, 131–146 (1995); L.-H. Wang, S. L. Jacques, and L.-Q. Zheng, ''CONV—Convolution for responses to a finite diameter photon beam incident on multi-layered tissues,'' *Comput. Methods Programs Biomed.* **54**, 141–150 (1997); http://biomed.tamu.edu/~lw
14. F. A. Duck, *Physical Properties of Tissue: A Comprehensive Reference Book*, Academic Press, San Diego, CA (1990).
15. S. J. Matcher, M. Cope, and D. T. Delpy, ''*In vivo* measurements of the wavelength dependence of tissue-scattering coefficients between 760 and 900 nm measured with time-resolved spectroscopy,'' *Appl. Opt.* **36**(1), 386–396 (1997).
16. W. G. Zijlstra, A. Buursma, and W. P. Meeuwsen-van der Roest, ''Absorption spectra of human fetal and adult oxyhemoglobin, de-oxyhemoglobin, carboxyhemoglobin, and methemoglobin,'' *Clin. Chem.* **37**(9), 1633–1638 (1991).
17. L. T. Perclman, V. Backman, M. Wallace, G. Zonios, R. Manoharan, A. Nusrat, S. Shields, M. Seiler, C. Lima, T. Hamano, I. Itzkan, J. Van Dam, J. M. Crawford, and M. S. Feld, ''Observation of periodic fine structure in reflectance from biological tissue: A new technique for measuring nuclear size distribution,'' *Phys. Rev. Lett.* **80**(3), 627–630 (1998).
18. B. C. Wilson, W. P. Jeeves, D. M. Lowe, and G. Adam, ''Light propagation in animal tissues in the wavelength range 375–825 nanometers,'' *Proceedings of the Clayton Foundation International Symposium on Porphyrin Localization and Treatment of Tumors*, pp. 115–132 (1983).